390–404 *Nucleic Acids Research, 2020, Vol. 48, No. 1* *Published online 12 November 2019*
doi: 10.1093/nar/gkz1073

A unique internal ribosome entry site representing a dynamic equilibrium state of RNA tertiary structure in the 5′-UTR of *Wheat yellow mosaic virus* RNA1

Guowei Geng, Chengming Yu, Xiangdong Li and Xuefeng Yuan *

Department of Plant Pathology, College of Plant Protection, Shandong Agricultural University, Shandong Province Key Laboratory of Agricultural Microbiology, Tai'an 271018, P.R. China

Received June 17, 2019; Revised October 23, 2019; Editorial Decision October 24, 2019; Accepted October 31, 2019

ABSTRACT

Internal ribosome entry sites (IRESes) were first reported in RNA viruses and subsequently identified in cellular mRNAs. In this study, IRES activity of the 5′-UTR in *Wheat yellow mosaic virus* (WYMV) RNA1 was identified, and the 3′-UTR synergistically enhanced this IRES activity via long-distance RNA–RNA interaction between $C^{80}U^{81}$and $A^{7574}G^{7575}$. Within the 5′-UTR, the hairpin 1(H1), flexible hairpin 2 (H2) and linker region (LR1) between H1 and H2 played an essential role in cap-independent translation, which is associated with the structural stability of H1, length of discontinuous stems and nucleotide specificity of the H2 upper loop and the long-distance RNA–RNA interaction sites in LR1. The H2 upper loop is a target region of the eIF4E. Cytosines (C^{55}, C^{66}, C^{105} and C^{108}) in H1 and H2 and guanines (G^{73}, G^{79} and G^{85}) in LR1 form discontinuous and alternative base pairing to maintain the dynamic equilibrium state, which is used to elaborately regulate translation at a suitable level. The WYMV RNA1 5′-UTR contains a novel IRES, which is different from reported IRESes because of the dynamic equilibrium state. It is also suggested that robustness not at the maximum level of translation is the selection target during evolution of WYMV RNA1.

INTRODUCTION

The effective translation of viral proteins is essential for the life cycle of viruses. Translation of the viral proteins in eukaryotes must rely on the translation machinery of the host, which prefers mRNAs with a 5′-cap and 3′poly (A) tail. The 5′-cap recruits a 40S ribosomal subunit through the binding of eIF4E, as well as a series of host factors such as eIF4G, which ensures the effective initiation of translation in the canonical cap- and scanning-dependent mechanism (1–3). Except to maintain the integrity of mRNA, 3′-poly (A) enhances translation efficiency through the cyclization of mRNA, which is mediated by a series of interactions of the 3′-poly(A)-PABP-eIF4G-eIF4E-5′-cap (4).

However, many RNA viruses contain genomic RNAs lacking the 5′-cap and/or 3′- poly(A). Two types of cap-independent translation *cis*-elements have been identified. One is located at the 5′-upstream of the corresponding ORFs and termed the internal ribosome entry site (IRES) (5). The other is located at the 3′-downstream of the corresponding ORF and termed the 3′-cap-independent translation elements (3′-CITE) (6,7). In spite of the different locations, both IRES and 3′-CITE can recruit a 40S ribosomal subunit in an indirect or direct manner to initiate end-independent translation by various mechanisms (5,7,8). 3′-CITE was first reported in satellite *Tobacco necrosis virus* (sTNV) (9) and was subsequently explored in plant RNA viruses (6,7). The 3′-CITE was recently identified in animal RNA viruses and host cellular mRNAs through a high-throughput bicistronic assay (10). IRES was first reported in picornavirus RNAs (11,12), and has been subsequently reported in many animal and plant viruses, as well as host cellular mRNAs (5,10,13–16).

For animal RNA viruses, viral IRESes have been reported mainly from the Picornaviridae family and also from the Dicistroviridae family, hepatitis C virus (HCV), and pestiviruses in the Flaviviridae family (17), and classified into six classes based on their characteristic structure and distinct mechanism promoting initiation involved in the requirement of various initiation factors and IRES *trans*-acting factors (ITAFs) (17,18). It consists of one type, i.e. IRES from the Dicistroviridae family and five types involved in IRESes mainly from the members of the Picornaviridae family (17). The intergenic region (IGR) IRESes of CrPV and PSIV in the Dicistroviridae family, consist of three pseudoknots and directly bind to the A site of the 40S ribosomal subunit mimicking a tRNA/mRNA interaction without the requirement of initiation factors (19,20). The other five types of IRESes contain multiple hairpins and form complicated tertiary structures and recruit a 40S ribo-

*To whom correspondence should be addressed. Tel: +86 538 8205608; Fax: +86 538 8242375; Email: snowpeak77@163.com

somal subunit via the assistance of various initiation factors and/or ITAFs (17,18,21–31). Nuclear magnetic resonance, X-ray crystallography and Cryo-EM reconstructions have been applied to decipher the 3D structure of viral IRESes, such as the dicistrovirus intergenic region and the HCV-like IRES (5,20,32,33). Based on IRES structural features, compounds or small molecules were designed to inhibit viral protein synthesis (34–39), which provide a new way to control viral diseases.

For plant RNA viruses, IRESes have been mainly identified in members of the Potyviridae family, such as *Tobacco etch virus* (TEV), *Turnip mosaic virus* (TUMV) and *Potato virus Y* (PVY), which require a cap-independent translation mechanism to facilitate polyprotein expression (16,40–42). However, there is much less known about IRES in plant viruses than in animal viruses. Compared with the high-level structure of the IRESes in animal RNA viruses, the structure of IRES in plant viruses is not as pronounced but usually has a weak secondary structure or few hairpins, which is responsible for the activity of the IRESes, and they may be classified as a new type of plant virus translation enhancer (16). For viruses encoding VPg, different structural characteristics of the IRESes between animal viruses and plant viruses may be associated with remarkable size differences in the VPg of the viruses (43), because the VPg may affect translation through the binding of the eIF4E and other ribosomal proteins (44,45). The *Bymovirus* genus is exclusive to the family of Potyviridae because of the bipartite genome. There has been no report on the cap-independent translation enhancer or IRESes in members of *Bymovirus*.

Wheat yellow mosaic virus (WYMV) is a member of the *Bymovirus* genus and causes severe losses in wheat production in East Asia, including China and Japan (46–49). Its symptoms are similar to diseased wheat caused by filamentous viruses transmitted by *Polymyxagraminis* in Europe, Asia and North America (49–51). The genome of WYMV comprised two (+) single-stranded RNAs. Both RNA1 and RNA2 code a polyprotein to produce functional proteins by proteinases (46,52,53). Nucleotide sequences of coding regions among different WYMV isolates present high identities whereas untranslated regions have a relatively higher mutation rate (54). Compared with the 5′-UTR of WYMV RNA2, the 5′-UTR of WYMV RNA1 has a higher homology among different WYMV isolates (54). In this study, IRES in the 5′-UTR of WYMV RNA1 was identified. Moreover, structure probing and mutagenesis assays suggested that a dynamic equilibrium state of the RNA tertiary structure is essential for the 5′-UTR of WYMV RNA1 to facilitate IRES activity at a suitable level.

MATERIALS AND METHODS

Construction of plasmids and preparation of DNA fragments

All plasmids were constructed based on the firefly luciferase (FLuc) reporter construct pT7-F-3′-UTRssp vector (55) via polymerase chain reaction (PCR) amplification, enzyme digestion, and ligation. All plasmids were confirmed by DNA sequencing. Detailed information concerning plasmid construction and names of corresponding *in vitro* transcripts are shown in Supplementary Table S1.

DNA fragments were amplified via PCR to be the template for preparing corresponding *in vitro* transcripts, which were used for the electrophoretic mobility shift assay (EMSA), in-line probing and *trans*-competition assays. Detailed information is shown in Supplementary Table S2.

In vitro translation

In vitro translation assays were performed as previously described (55). Briefly, the *in vitro*-synthesized RNA transcripts (3 pmol) corresponding to designated translation reporter constructs were used in a 25-μl translation reaction using wheat germ extract (WGE) (Promega) according to the manufacturer's instructions. The luciferase activity was measured using a luciferase assay reporter system (Promega) and a Modulus Microplate Multimode Reader (Turner BioSystems). At least three independent *in vitro* translation assays were performed for each construct. Standard errors were calculated in Microsoft Excel. Statistical analyses of the significance of *in vitro* translation assays were performed using SPSS or *t*-test, as indicated (56).

In-line probing

In-line structure probing was performed as previously described (57). Briefly, RNA fragments of the WYMV RNA1 5′-UTR (positions 1–162) or the WYMV RNA1 partial 3′-UTR (positions 7500–7644) were separately 5′end-labeled with [γ-32P]ATP and denatured at 75°C, followed by slowly cooling to 25°C. RNA was incubated at 25°C in 50 mM Tris–HCl (pH 8.5) and 20 mM $MgCl_2$ for 14 h. To identify potential RNA–RNA interaction, unlabeled candidate RNA fragments were co-incubated with isotope-labeled RNA fragments. Samples were separated by 8% polyacrylamide gel electrophoresis (8 M urea) alongside a hydroxide-generated RNA cleavage ladder and RNase T1 digestion product on labeled RNA fragments. Then, the gels were dried and exposed to a phosphorimager screen, followed by detection with the Typhoon FLA 7000 (GE Healthcare). At least two independent in-line probing assays were performed for each fragment.

Signals of the in-line probing reaction were analyzed as following: first, reaction signals of nucleotides in stem regions predicted by mFold (http://unafold.rna.albany.edu/?q=mfold/RNA-Folding-Form2.3) were designated as the background band; then, reaction signals of nucleotides in other regions were compared to the background band to determine the difference (strong/weak/no difference). Strong or weak signals compared to those of the background band were indicated by red or green solid arrows on gels and red or green nucleotides in the structure figures. When there were several in-line probing reactions, green hollow triangles point to the weaker cleavage sites, whereas red hollow triangles point to the stronger cleavage sites compared within corresponding sites in the wild-type (wt) RNA1 5′-UTR.

Electrophoretic mobility shift assay

EMSA were used to test the interaction sites between the 5′-UTR and 3′-UTR of WYMV RNA1. The 5′end-labeled

5′-UTR or 3′-UTR of WYMV RNA1 (AF067124) was used for a 10.0-μl reaction volume, which also included 50-fold of unlabeled competing RNA fragments at 75°C for denaturation-natural refolding treatment; when the temperature reached room temperature (25°C), the treatment was complete. Subsequently, 10.0 μl of 2 × RNA binding buffer (10 mM HEPES, pH 7.9, 200 mM KCl, 10 mM $MgCl_2$ and 7.6% glycerol) was added to the reaction solution at 25°C for 0.5 h, and 5.0 μl of RNA–RNA EMSA loading buffer (2.5 μl of 2 × RNA binding buffer, 2.5 μl of 100% glycerol, 0.001 g of xylenecyanol FF and 0.001 g of bromophenol blue) was added to the reaction solution. The reaction products were separated by 5% native polyacrylamide gel electrophoresis. Then, the gels were dried and exposed to a phosphorimager screen, followed by detection with the Typhoon FLA 7000 (GE Healthcare).

eIF4E expression and purification

The eIF4E coding sequence (KX467331) of wheat was amplified by RT-PCR and inserted into a pEHisTEV vector through the enzyme sites BamH I and Sal I. The positive plasmid containing eIF4E (KX467331) was transformed into *Escherichia coli* Rosetta. The eIF4E proteins were expressed under the induction of 0.5 M isopropyl-β-D-thiogalactoside (IPTG) at 37°C for 5 h. Samples were separated by sodium dodecyl sulphate-polyacrylamide gelelectrophoresis (SDS-PAGE). The gel bands containing the 24 kDa eIF4E were cut and placed into dialysis bags. After 2 h of electrophoresis in SDS-PAGE buffer, the gel in the dialysis bags was removed and the dialysis bags were dialyzed for 24 h followed by split charging of the eIF4E proteins.

Trans-competition assay

The *trans*-competition assay was performed based on the *in vitro* translation assay to test the effect of the additional competing items including 1.6 mM cap analog/1.6 mM magnesium ($MgCL_2$), 6 mM eIF4E, 50-fold or 100-fold RNA fragments and 8 μM oligonucleotides.

RNA stability assay

RNA stability assays were measured by testing the RNA status after 1.5 h of *in vitro* translation assay using northern blotting. Sequences of the specific probe for northern blotting were 5-acgtgatgttcacctcgatatgtgcatctg-3, which is complemented with the coding region of the firefly luciferase (FLuc) gene.

RESULTS

5′-UTR of WYMV RNA1 presents IRES activity, which is synergistically enhanced by the 3′-UTR

To test the effect of the 5′-UTR of WYMV RNA1 on translation, RNA1 5′UTRs of three different WYMV isolates were respectively inserted upstream of the FLuc gene (Figure 1A and B) and *in vitro* translation of the corresponding transcripts was evaluated using WGE. The 5′-UTRs of different WYMV RNA1 (AF067124, KX258948 and KX258947) enhanced the translation of FLuc to 6- to 8-fold in the absence of the 5′cap, which showed cap-independent translation enhancement activity (Figure 1B). Furthermore, the cap-independent translation enhancement activity of the 5′-UTR of WYMV RNA1 (AF067124) could be enhanced to 3.15-fold in the presence of the RNA1 3′UTR, although the RNA1 3′-UTR could not enhance the translation of FLuc by itself (Figure 1C). In addition, the cap-independent translation enhancement activity of the WYMV RNA1 5′-UTR was not affected by the insertion of adjacent downstream 60 nt coding sequences (Figure 1D), suggesting that the 5′-UTR of WYMV RNA1 contained the inherent sequence and structure characteristically responsible for the cap-independent translation enhancement. When a long stem-loop (SL) was added upstream, the 5′-UTR of WYMV RNA1 still enhanced the translation to 2.8-fold that of the control vector (F) (Figure 1D), indicating that the 5′-UTR of WYMV RNA1 presents IRES activity. In addition, the 5′-UTR of WYMV RNA1 also enhanced the translation to 6.5-fold in the presence of the 5′cap (Figure 1D). To map the boundaries of the IRES in the 5′-UTR of WYMV RNA1, a series of deletion mutations from the 5′end or 3′end within the 5′-UTR were constructed (Supplementary Figure S1). After deletions of 20 nt from the 5′end (F-R1-5U-5′△20) or 30 nt from the 3′end (F-R1-5U-3′△30), the translation of constructs remained at more than 70% of that of the wt F-R1-5U. However, deletions of 30 nt from the 5′end (F-R1-5U-5′△30) or 40 nt from the 3′end (F-R1-5U-3′△40) caused translation <50% of that of the wt F-R1-5U (Supplementary Figure S1). Further deletion of 10 nt from position 20 or 130 caused a sharp loss of translation (Supplementary Figure S1). It is suggested that the core elements of IRES within the 5′-UTR of WYMV RNA1 are mainly located from position 20 to position 130.

Long-distance RNA–RNA interaction between 5′-UTR and 3′-UTR enhances the IRES activity of WYMV RNA1 5′-UTR

The phenomenon of the RNA1 3′-UTR enhancing IRES activity of the RNA1 5′-UTR may have resulted from a potential RNA–RNA interaction between the 5′-UTR and 3′-UTR of WYMV RNA1 (Figure 1C). To identify the potential long distance RNA–RNA interaction between the 5′-UTR and 3′-UTR, structures of the RNA1 5′-UTR were analyzed in the absence or presence of the RNA1 3′-UTR via in-line probing assay (Figure 2A). RNA1 5′-UTR has two hairpins (H1 and H2) based on the in-line cleavage pattern (Figure 2A and B). In the presence of the 3′-UTR, the linker region (LR1) between H1 and H2 showed reduced in-line cleavage in three discontinuous parts (Figure 2A and B), which implies new-forming base pairing because of the presence of the 3′-UTR. Other changed characteristics of the 5′-UTR structure may be a consequence of the potential base pair between the LR1 and the 3′-UTR.

To map the interaction sites in LR1 forming base pairs with and the 3′-UTR of WYMV RNA1, EMSA between 5′-UTR or LR1 mutants and 3′-UTR was performed (Figure 3A and B). The wt RNA1 5′-UTR, LRm1 and LRm3 interacted with the RNA1 3′-UTR, whereas LRm2

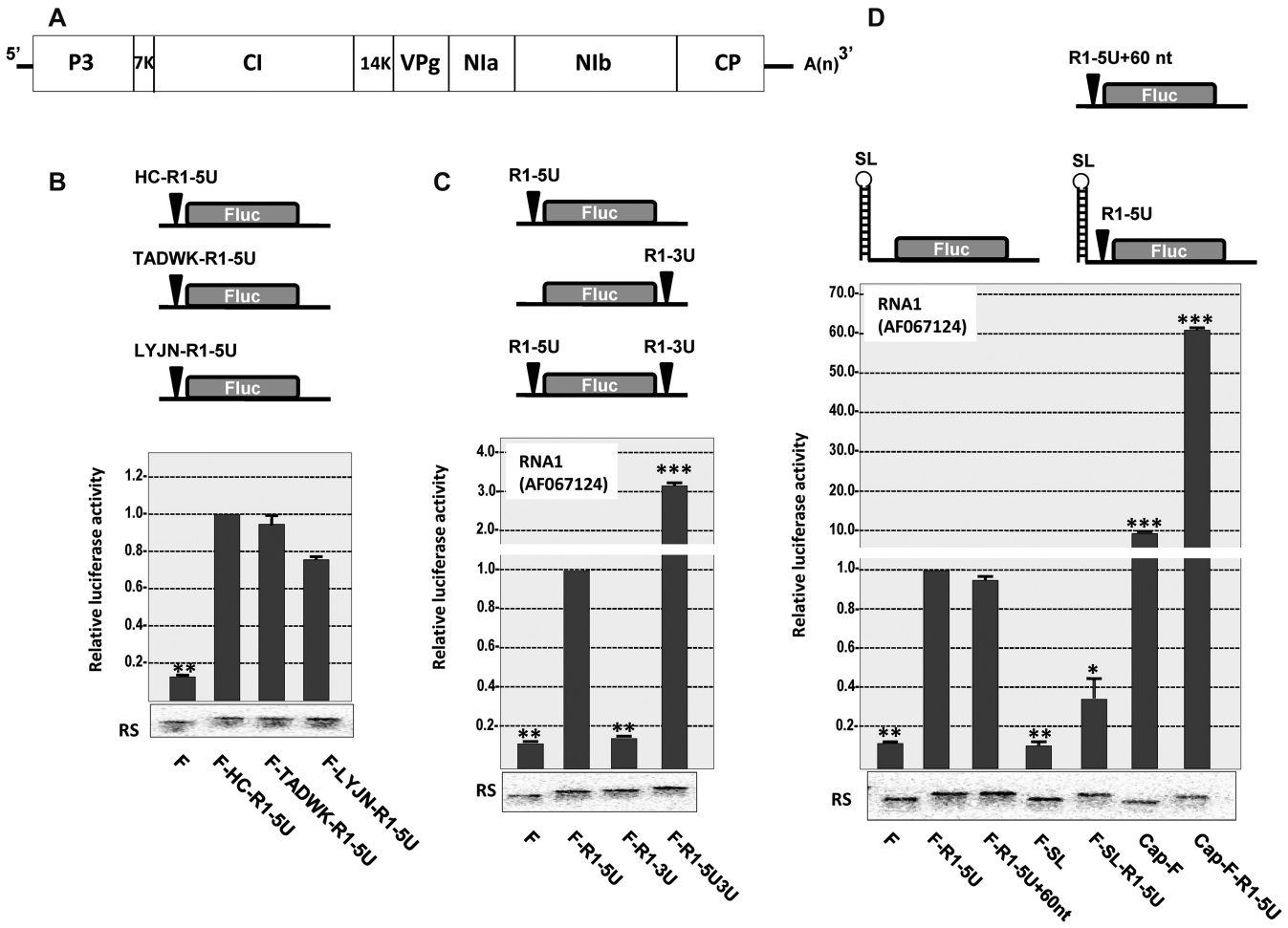

Figure 1. Effect of the UTRs of *WYMV* RNA1 on translation. (**A**) Genome organization of WYMV RNA1. (**B**) Effects of the RNA1 5′-UTR of three WYMV isolates on translation. FLuc, firefly luciferase; F, vector control; HC, Huangchuan isolate (RNA1 accession number: AF067124); TADWK, Taian isolate (RNA1 accession number: KX258948); LYJN, Linyi isolate (RNA1 accession number: KX258947); R1, RNA1; 5U, 5′-UTR. (**C**) Effects of the 5′-UTR and 3′-UTR of WYMV RNA1 (AF067124) on translation. 3U, 3′-UTR. (**D**) Effects of the 5′-UTR of WYMV RNA1 (AF067124) in the presence of the downstream coding region, additional upstream stem-loop, or 5′-cap structure. SL, stem-loop. * indicates $P < 0.05$, ** $P < 0.01$, *** $P < 0.001$; RS indicates RNA stability assay after 1.5 h *in vitro* translation.

($C^{80}U^{81}$→GA) failed to interact with the 3′-UTR (Figure 3B). It is suggested that $C^{80}U^{81}$ in the LR1 of 5′-UTR are one side of the interaction sites between the 5′-UTR and 3′-UTR of WYMV RNA1.The effect of this RNA–RNA interaction between the 5′-UTR and 3′-UTR of RNA1 on translation was analyzed through mutagenesis of the FLuc reporter constructs (Figure 3C). In the construct with both 5′-UTR and 3′-UTR (F-R1-5U3U), mutation of $C^{80}U^{81}$ to GA (LRm2) reduced translation to a level comparable to that of the construct with 5′-UTR itself (F-R1-5U). LRm2 in F-R1-5U slightly reduced the translation (Figure 3C). It is suggested that the mutation of $C^{80}U^{81}$ to GA ploughed under the additive effect of the 3′-UTR on the IRES activity of the 5′-UTR. In addition, the mutation of LRm1 reduced the translation of F-R1-5U3U to 56%, primarily because of its negative effect on the IRES activity of the 5′-UTR, because LRm1 in F-R1-5U reduced the translation to 54% of that of the wt (Figure 3C). Mutation of LRm3 slightly reduced the translation of F-R1-5U3U and remarkably increased the translation of F-R1-5U to 2-fold (Figure 3C). It is conclusive that $C^{80}U^{81}$ in the LR1 mediated the interaction between the 5′-UTR and 3′-UTR, which further enhanced the IRES activity of the 5′-UTR of WYMV RNA1.

To map the interaction sites in 3′-UTR forming base pairs with LR1 of the 5′-UTR of WYMV RNA1, the structure of the 3′terminal regions of RNA1 was also analyzed by in-line probing, which showed that the 3′ terminal regions of RNA1 contain several hairpins (Figure 4A and B). Based on the in-line cleavage pattern, three clusters of AG, which may potentially form base pairs with $C^{80}U^{81}$ in LR1 of the 5′-UTR, were selected and tested through mutagenesis and EMSA (Figure 4). Mutation of $A^{7574}G^{7575}$ to UC (m7574) in the 3′UTR failed to interact with the 5′-UTR of RNA1 based on EMSA, while the wt 3′-UTR, 3′-UTR mutation of $A^{7539}G^{7540}$ to UC (m7539) and 3′-UTR mutation of $A^{7635}G^{7636}$ to UC (m7635) still interacted with the 5′-UTR of RNA1 (Figure 4B and C). Mutation of $A^{7635}G^{7636}$ to UC (m7635) remarkably increased the translation to 1.67-fold that of F-R1-5U3U (Figure 4D). It is suggested that $A^{7635}G^{7636}$ may inhibit the interaction efficiency between

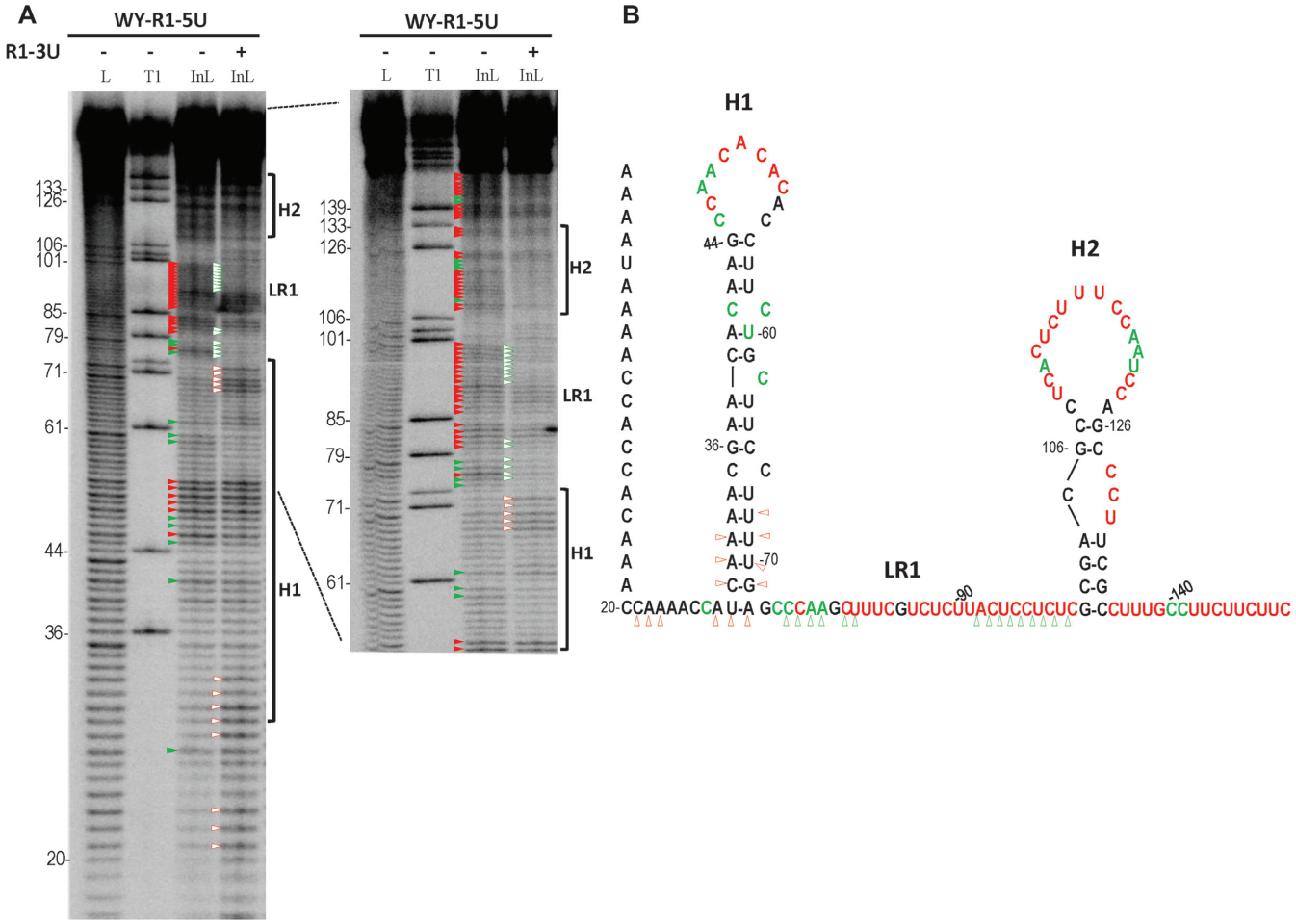

Figure 2. Structure probing of the 5′-UTR of WYMV RNA1 in the absence or presence of the RNA1 3′-UTR. (**A**) In-line probing of WYMV RNA1 5′-UTR in the absence or presence of the RNA1 3′-UTR. L, ladder generated from treatment with NaOH; T1, ladder generated from fragment denaturation and treatment with RNase T1, which cleaves at guanylates. InL, in-line cleavage products. Base numbering is at the left of the panel and positions of hairpins (H) and linker region (LR) are noted to the right. Red and green solid triangles point to strongly marked and marked cleavage sites in the RNA1 5′-UTR, respectively. Green hollow triangles point to the weaker cleavage sites, whereas red hollow triangles point to the stronger cleavage sites within the RNA1 5′-UTR in the presence of RNA1 3′-UTR versus the absence of RNA1 3′-UTR. H1, hairpin 1; H2, hairpin 2; LR1, linker region 1. (**B**) RNA structure of WYMV RNA1 5′-UTR in the absence or presence of the RNA1 3′-UTR. Black, green and red nucleotides respectively indicate none or inapparent, marked and strongly marked cleavage based on the in-line probing pattern. Green and red nucleotides indicate the single-strand characteristics. Green hollow triangles point to the weaker cleavage sites, whereas red hollow triangles point to the stronger cleavage sites within the RNA1 5′-UTR in the presence of RNA1 3′-UTR.

3′-UTR and 5′-UTR through the local tertiary structure of the 3′-UTR in the background of the wt RNA1. Mutation of $A^{7574}G^{7575}$ to UC (m7574) reduced translation to 48% of that of F-R1-5U3U, while simultaneous mutation of $A^{7574}G^{7575}$ to UC (m7574) and mutation of $C^{80}U^{81}$ to GA (LRm2) in F-R1-5U3U can rescue the translation to 67% of that of F-R1-5U3U (Figure 4D). It is concluded that $A^{7574}G^{7575}$ is complementary with $C^{80}U^{81}$ and mainly mediated interaction between the 3′-UTR and the 5′-UTR of WYMV RNA1, which is responsible for the synergistical enhancement of translation. Alignment data of 5′-UTR and 3′-UTR of different WYMV RNA1 suggested that the long-distance interaction was conserved, which maintained the reverse base pairing between $(C/U)^{80}U^{81}$ and $(A/G)^{7574}G^{7575}$ although the nucleotide at position 80 or position 7574 in a fraction of WYMV RNA1 was changed (Supplementary Figure S2). Structures of LRm2 in the absence or presence of 3′-UTR-m7574 were probed by in-line probing to further confirm the long-distance interaction between $C^{80}U^{81}$ and $A^{7574}G^{7575}$ (Supplementary Figure S3). Although LRm2 caused some enhanced cleavages on single-strand nucleotides in different regions (Supplementary Figure S3), it did not change the structure pattern of the 5′-UTR. LRm2 made the whole structure of the 5′UTR more identical. In the presence of 3′UTR-m7574, LRm2 almost restored the cleavage pattern to that of wt 5′-UTR, except for the confinement of ^{80}GA by ^{7574}UC (Supplementary Figure S3). It is further suggested that the long-distance RNA–RNA interaction between ^{80}CU and ^{7574}AG occurs in the wt WYMV RNA1.

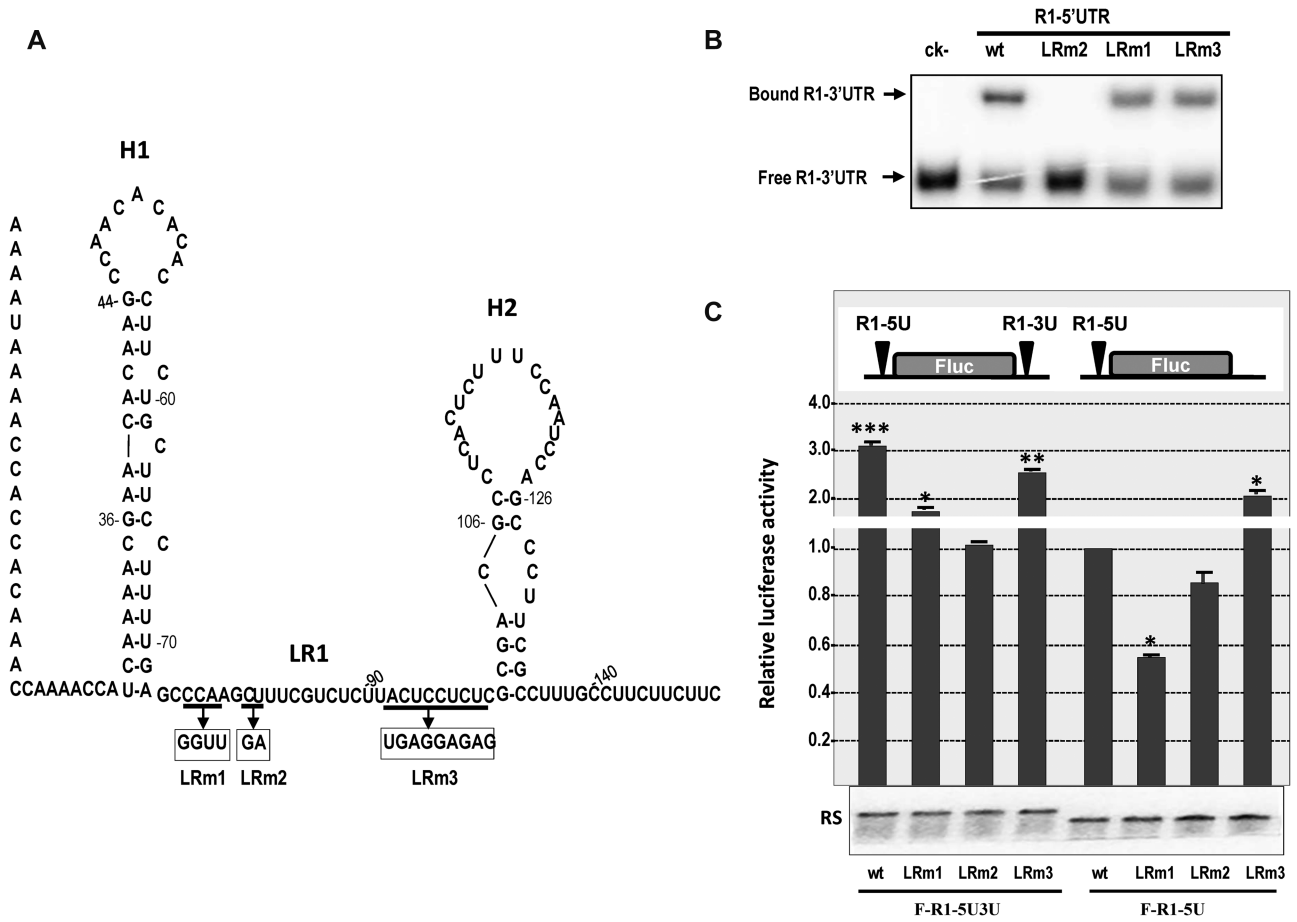

Figure 3. Mapping of sites in 5′-UTR forming RNA–RNA interaction with 3′-UTR in WYMV RNA1. (**A**) Mutations on potential RNA–RNA interaction sites within 5′-UTR of WYMV RNA1. H1, hairpin 1; H2, hairpin 2; LR1, linker region 1. (**B**) EMSA analysis between RNA1 5′-UTR or its mutants and RNA1 3′-UTR. (**C**) Effects of mutations of potential RNA–RNA interaction sites on the translation of the reporter gene. * indicates $P < 0.05$, ** $P < 0.01$, *** $P < 0.001$; RS indicates RNA stability assay after 1.5 h *in vitro* translation.

Key characteristics of H1 and H2 involved in IRES activity of the 5′-UTR of WYMV RNA1

Based on the in-line cleavage pattern, WYMV RNA1 has two hairpins (H1 and H2) in the 5′-UTR (Figure 2A and B). The linker region (LR1) between them played key roles in the long-distance RNA–RNA interaction between the 5′-UTR and 3′-UTR of WYMV RNA1, which have additive effects on the IRES activity of the RNA1 5′UTR (Figure 3). Based on the deletion mutation data of the 5′-UTR, the core element of IRES could be located at H1, H2, and LR1 (Supplementary Figures S1 and 2). Mutagenesis was performed to test the effect of H1 and H2 on the IRES activity of the 5′-UTR (Figure 5).

For the long stem of H1, mutations of the middle region (MS2, MS3 and MS4) reduced translation to 74, 41 and 37% of that of the wt F-R1-5U, whereas mutations of the terminal regions (MS1 and MS5) slightly enhanced translation compared to that of the wt F-R1-5U (Figure 5A and B). MS3 and MS4 caused changes in the cleavage pattern of the stem of H1 and did not misfold other regions (Supplementary Figure S4); thus, the stability of the main structure of the long stem of H1 was essential for the IRES activity of the 5′-UTR. For the top loop of H1, the mutation of $A^{54}C^{55}$ to UG (ML4) reduced the translation to 16% of that of F-R1-5U, whereas the other three mutations in the top loop (ML1, ML2 and ML3) slightly affected the IRES activity of the 5′-UTR (Figure 5A and B). It is suggested that the stability of the long stem and nucleotide specificity of $A^{54}C^{55}$ is the core characteristic of H1 involved in IRES activity of the 5′-UTR of WYMV RNA1.

For H2, mutations breaking the base pairing of discontinuous stems (MS6 and MS7) had no effect on the IRES activity of the 5′-UTR (Figure 5A and C). However, deletion mutations of discontinuous stems (DS1 and DS2) decreased the translation to lower than 20% of that of the wt (Supplementary Figure S5). The stability of discontinuous stems of H2 is not critical, but the length of discontinuous stems of H2 is critical for IRES activity, so H2 is flexible, which may provide suitable flexibility and space to allow core elements of H2 to play an important role. Mutation of the middle loop (ML5) increased the translation to 1.5-fold that of F-R1-5U (Figure 5A and C). Different mutations in the top loop of H2 presented entirely different effects on translation. ML6 and ML7 decreased the translation to 45 and 24% of that of F-R1-5U, respectively, whereas ML8 increased the translation to 2.1-fold that of F-R1-5U (Fig-

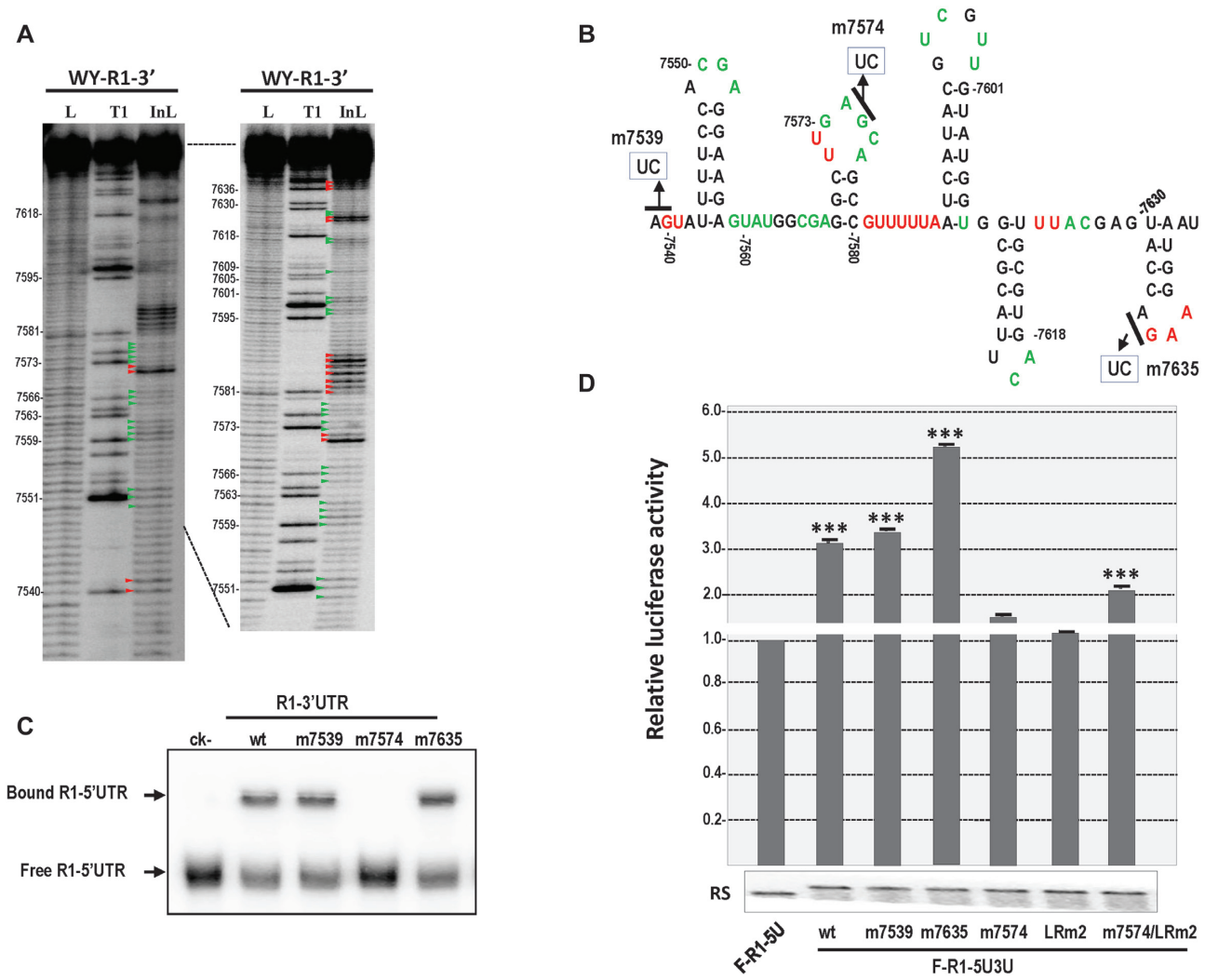

Figure 4. Mapping of sites in the 3′-UTR forming RNA–RNA interaction with LR1 of the 5′-UTR in WYMV RNA1. (**A**) In-line probing of WYMV RNA1 3′-UTR. The legend is similar to that of Figure 2A. (**B**) RNA structure of WYMV RNA1 3′-UTR. The legend is similar to that of Figure 2B. (**C**) EMSA analysis between RNA1 3′-UTR or its mutants and RNA1 5′-UTR. (**D**) Effects of mutations of potential RNA–RNA interaction sites on the translation of the reporter gene. * indicates $P < 0.05$, ** $P < 0.01$, *** $P < 0.001$; RS indicates RNA stability assay after 1.5 h *in vitro* translation.

ure 5A and C). ML6 and ML7 caused a change in the cleavage pattern of the top loop of H2 and did not misfold other regions; thus, the nucleotide specificity for the top loop of H2 is the core characteristic of H2 involved in the IRES activity of the 5′-UTR of WYMV RNA1.

IRESes reported previously can recruit a 40S subunit directly or indirectly through binding translation initiation factors, such as eIF4E (16,17). A competitive assay was performed to test the potential requirement on eIF4E during *in vivo* translation mediated by the 5′-UTR of WYMV RNA1 (Figure 6). In the presence of the 1.6 mM dissociative cap analog/Mg^{2+}, the IRES activity of the RNA1 5′-UTR failed to exert, which is revealed through the translation of F-5U, which is even lower than that of the basic vector (F) (Supplementary Figure S6 and Figure 6A). However, the confined IRES activity of RNA1 5′-UTR by the cap analog/Mg^{2+} was rescued to 62% of that of the wt through the addition of eIF4E (Figure 6). It is suggested that the IRES activity of the 5′-UTR of WYMV RNA1 is in an eIF4E-dependent manner. Furthermore, a competitive assay was also used to map the potential target region of eIF4E within RNA1 5′-UTR. Based on the previous mutagenesis assay, LRm1, ML6 and ML7 were selected because of their remarkable negative effect on the IRES activity of the 5′-UTR of WYMV RNA1 (Figures 3 and 5). In the presence of the dissociative cap analog/Mg^{2+} and additive eIF4E, the competition activity of RNA fragments was wt > LRm1 > ML6 > ML7, which is supported by the translation level of F-5U presenting ML7 > ML6 > LRm1 > wt (Figure 6A). The wt R1-5U presented a high competition activity on eIF4E, which is revealed by the translation level of F-5U compared to the background level. ML7 in R1-5U almost lost the competition on eIF4E, which is revealed by the translation level being 79% of that of the uncompetitive status. ML6 in R1-5U also lost partial competition on eIF4E. In the absence of the cap analog/Mg^{2+} and additive eIF4E, ML7 and ML6 presented similar patterns of the competition capacity (Figure 6A). In addition,

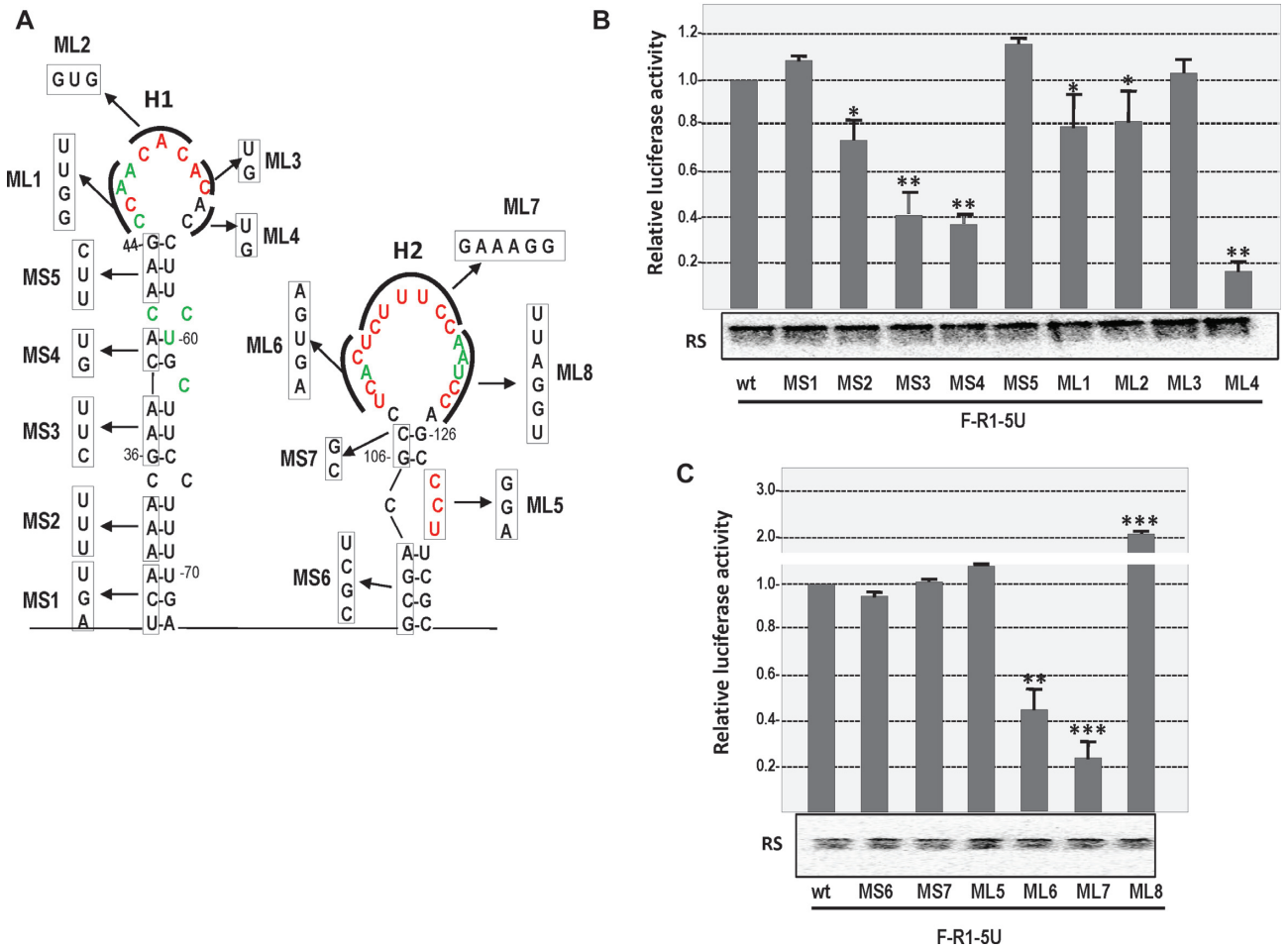

Figure 5. Core *cis*-elements within H1 and H2 involved in cap-independent translation. (**A**) Mutations within H1 and H2. (**B**) Effects of mutations of H1 on the cap-independent translation of the FLuc. (**C**) Effects of mutations of H2 on the cap-independent translation of the FLuc. * indicates $P < 0.05$, ** $P < 0.01$, *** $P < 0.001$; RS indicates RNA stability assay after 1.5 h *in vitro* translation.

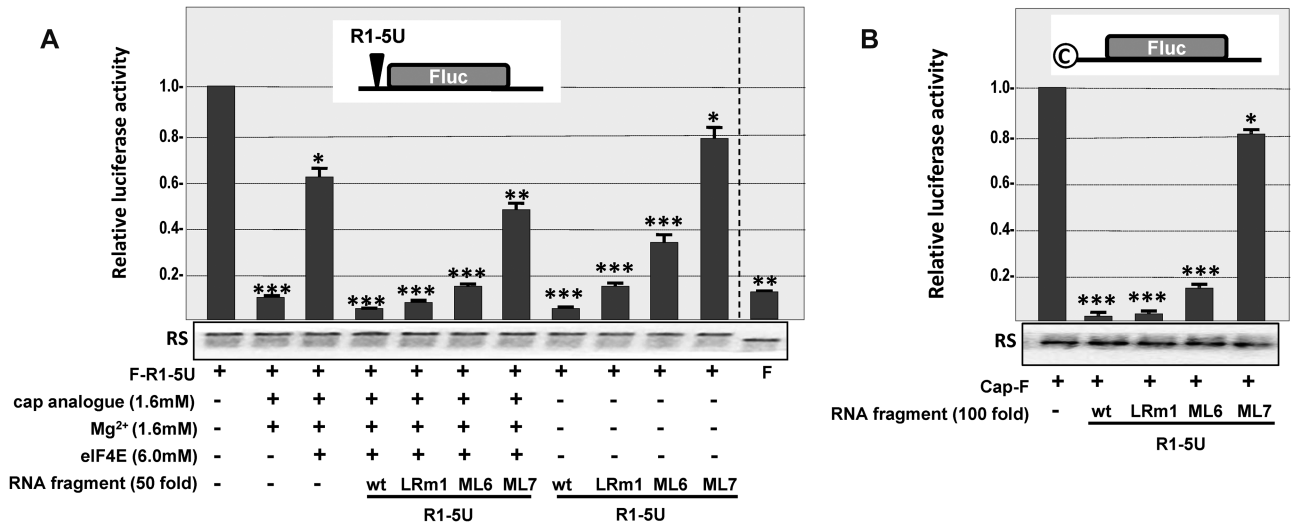

Figure 6. Mapping of eIF4E target regions within the 5′-UTR of WYMV RNA1. (**A**) Competition on translation mediated by the 5′-UTR of WYMV RNA1 from dissociative cap analog, eIF4E and/or 5′-UTR fragments. (**B**) Competition on translation mediated by the 5′-cap from dissociative 5′-UTR fragments. * indicates $P < 0.05$, ** $P < 0.01$, *** $P < 0.001$; RS indicates RNA stability assay after 1.5 h *in vitro* translation.

these 5′-UTR RNA fragments presented similar patterns in terms of the competition capacity on the translation mediated by the 5′cap (Figure 6B). It is suggested that the target site of the eIF4E within the 5′-UTR of WYMV RNA1 is the top loop of H2 (Figure 5A), especially the upper part (C^{114}UUUCC) of H2.

Tertiary equilibrium state ensures the IRES activity of the 5′-UTR of WYMV RNA1

Based on the above mutagenesis and competitive assays, an eIF4E-dependent pattern and core secondary elements of the IRES activity of RNA1 5′-UTR were identified. In addition to these core secondary elements, there are potential tertiary elements because there are several uncleaved cytosines (C^{35}, C^{55}, C^{66}, C^{105}, C^{108}) in the loop regions of H1 and H2 and guanines (G^{73}, G^{79}, G^{85}) in LR1 based on the in-line probing assay, which implied the potential discontinuous tertiary base pairs under the basis of H1, H2 and LR1 (Figures 2 and 7).

In the top loop of H1, a mutation of uncleaved AC to UG (ML4) reduced the translation to 16% of that of the wt (Figure 5A and B). Single-site mutations of A54U, C55G, C55A and C55U reduced the translation to 43, 27, 31 and 28% of that of the wt, respectively (Figure 7A and B). Thus, the nucleotide specificity of C^{55} is essential for IRES activity, which is possibly caused by the base pair with a special guanine in the tertiary structure of the RNA1 5′-UTR. In the middle region of the stem of H1, there are two uncleaved cytosines (C^{35} and C^{66}) surrounded by a long base pairing stem. Two mutations (C35G and C66G) were constructed to identify the effects of C^{35} and C^{66} on translation. The mutation of C35G and C66G had remarkably different effects on translation, although both of two mutations seemed to form base pairs between position 35 and 66. C35G had a slight effect on translation, whereas C66G reduced the translation to 11% of that of the wt. In addition, C66A and C66U reduced translation to 28 and 41% of that of the wt, respectively (Figure 7A and B). It is suggested that uncleaved C^{35} and C^{66} do not form the direct base pairs through non-Watson-Crick base pairing in the long stem of H1. It is also suggested that the nucleotide specificity of C^{66} is essential for IRES activity, which is possibly caused by base pairing with the special guanine in the tertiary structure of the RNA1 5′-UTR.

In H2, there are two uncleaved cytosines (C^{105} and C^{108}) in the single-strand regions. A single-site mutation of both increased translation to approximately 2-fold of that of wt 5′-UTR (Figure 7A and B). It is implied that C^{105} and C^{108} negatively regulated the IRES activity, which may be caused by base pairing with the special guanine in the tertiary structure of RNA1 5′-UTR.

In LR1, between H1 and H2, there are three discontinuous uncleaved guanines (G^{73}, G^{79}, and G^{85}), which implies potential base pairing with some special cytosines. Single-site mutations on them (G73C, G79C and G85C) had slight effects on translation, whereas the double-site mutations (G73C/G79C, G73C/G85C and G79C/G85C) reduced the translation to 32, 26 and 15% of that of the wt (Figure 7A and C), respectively. It is suggested that the inherent IRES activity of the RNA1 5′-UTR relies on the existence of at least two uncleaved guanines of G^{73}, G^{79} and G^{85}in LR1.

Based on the mutagenesis of these uncleaved cytosines and guanines in H1, H2 and LR1, it is suggested that C^{55}, C^{66}, C^{105}, C^{108}, G^{73}, G^{79} and G^{85} are essential for the inherent IRES activity of the 5′-UTR of WYMV RNA1 in different manners. We proposed the following hypotheses: (i) uncleaved cytosines (C^{55}, C^{66}, C^{105} and C^{108}) in H1 and H2 form dynamic base pairs with the three uncleaved guanines (G^{73}, G^{79} and G^{85}) in LR1; (ii) dynamic base pairs between uncleaved C^{55} and C^{66} in H1 and uncleaved guanines (G^{73}, G^{79} and G^{85}) in LR1 have positive effects on the IRES activity of the RNA1 5′-UTR; (iii) dynamic base pairs between uncleaved $C^{105}$and C^{108} in H2 and uncleaved guanines (G^{73}, G^{79} and G^{85}) in LR1 negatively regulate the IRES activity of the RNA1 5′-UTR; and (iv) dynamic base pairs among uncleaved cytosines (C^{55}, C^{66}, C^{105}, C^{108}) in H1/H2 and uncleaved guanines (G^{73}, G^{79} and G^{85}) in LR1 maintain a tertiary equilibrium state to ensure the IRES activity of the RNA1 5′-UTR at a suitable level. Multi-site mutation analyses were used to confirm the above hypotheses. Hexa-site mutations (C35G/C55G/C66G/G73C/G79C/G85C), which could transform potential base pairs between uncleaved cytosines in H1 and uncleaved guanines in LR1, rescued the translation to 89% of that of the wt, although single-site mutations (C55G, C66G) or double-site mutations (G73C/G79C, G73C/G85C and G79C/G85C) severely reduced translation (Figure 7D), which confirmed the potential base pairing among C^{55} and C^{66} in H1 and G^{73}, G^{79} and G^{85} in LR1. In addition, octonary-site mutation (C35G/C55G/C66G/G73C/G79C/G85C + C105G/C108G) reduced the translation to 68% of that of the wt, although C105G/C108G increased the translation to 2.22-fold that of the wt (Figure 7D), which confirmed the negative effect of uncleaved C^{105} and C^{108} on the IRES activity of the RNA1 5′-UTR.

To further identify the structural characteristics of the tertiary equilibrium state among these discontinuous C-G base pairs, in-line probing was performed to analyze the structure of mutants on these nucleotides (Figure 8A and B). The RNA structure of five mutants on the 5′-UTR of WYMV RNA1 was compared to that of the wt 5′-UTR. In general, mutants C(105/108)→G and m(5C→G+3G→C) showed remarkable consequential structural changes in addition to the structural change of the discontinuous nucleotides (Figure 8A and B). For the mutant C(105/108)→G, the top loop and upper part of the long stem in H1 showed enhanced in-line probing cleavage, which implied an unstable structure of this part compared to that in the wt. For the octonary-site mutant m(5C→G+3G→C), nucleotides involved in discontinuous C-G base pairs maintained similar cleavage patterns to those in the wt, except for the G^{105}, because of local base pairing with cytosine in the middle loop of H2 (Figure 8A and B). This indirectly suggests the existence of discontinuous base pairs among C^{55}, C^{66}, C^{105}, C^{108}, G^{73}, G^{79} and G^{85}. Furthermore, some nucleotides in the loop of H1, loop of H2 and 3′part of LR1 showed enhanced in-line cleavage in the octonary-site mutant m(5C→G+3G→C). It is further implied that the potential local base pairing of these nucleotides involved in discontinuous C-G base pair-

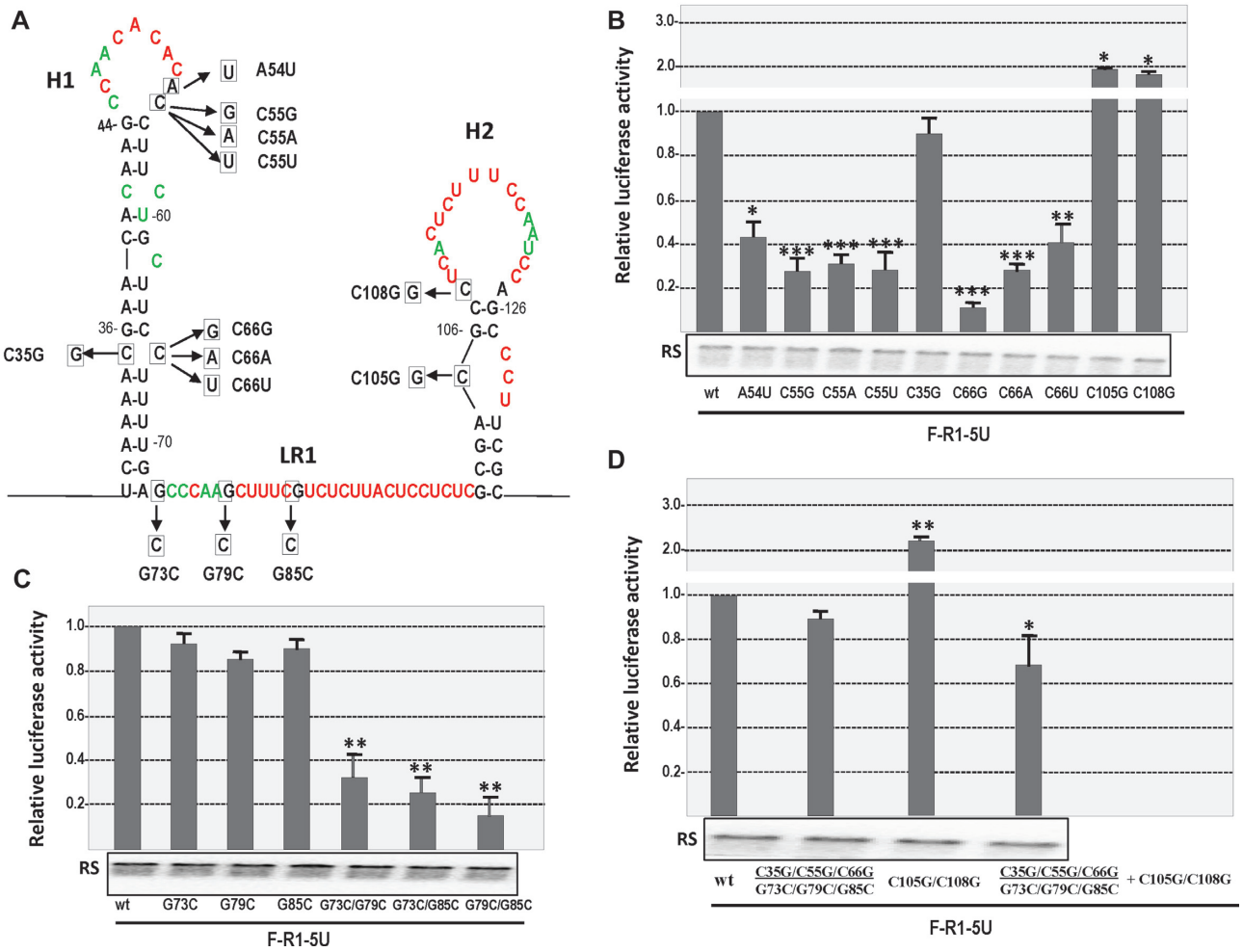

Figure 7. Potential discontinuous base pairs among several cytosines (C) in H1/H2 and guanines (G) in LR1. (**A**) Site mutations of several cytosines (C) in H1/H2 and guanines (G) in LR1. (**B**) Effects of site mutations within H1 and H2 on cap-independent translation. (**C**) Effects of site mutations of guanine (G) within LR1 on cap-independent translation. (**D**) Effects of simultaneous mutations of several cytosine(C) in H1/H2 and guanine(G) in LR1 on cap-independent translation. * indicates $P < 0.05$, ** $P < 0.01$, *** $P < 0.001$; RS indicates RNA stability assay after 1.5 h *in vitro* translation.

ing is also reflected by the structure probing patterns in mutants C(35/55/66)→G and G(73/79/85)→C (Figure 8A and B).

Based on all data of cap-independent translations mediated by the RNA1 UTRs of WYMV and structure probing (Figures 1–8), a model was proposed (Figure 9A). The IRES activity in WYMV RNA1 is in an eIF4E-dependent manner and the target site of eIF4E is located at the top loop of H2 (Figure 9A). The core tertiary characteristics of IRES activity are the tertiary equilibrium state mediated by an alternative interaction among C^{55} and C^{66} in H1; C^{105} and C^{108} in H2; and G^{73}, G^{79} and G^{85} in LR1 (Figure 9A). Interactions among C^{55} and C^{66} in H1 and G^{73}, G^{79} and G^{85} in LR1 positively regulate cap-independent translation, whereas interactions among C^{105} and C^{108} in H2 and G^{73}, G^{79} and G^{85} in LR1 negatively regulate cap-independent translation (Figure 9B). In addition, the IRES activity of the RNA1 5′-UTR was enhanced in the presence of the 3′-UTR through the long-distance RNA–RNA interaction between $C^{80}U^{81}$ and $A^{7574}G^{7575}$ (Figure 9A). The LR1 region is the scaffold and is responsible for not only the long-distance RNA–RNA interaction between 5′-UTR and 3′-UTR, but also the tertiary equilibrium state.

At last, a series of oligonucleotides complementary with different regions of RNA1 5′-UTR were used to evaluate their *trans*-effects on the translation mediated by the UTRs of WYMV RNA1 (Figure 10). They had negative effects on the translation of F-R1-5U3U to different extents. P1 (agc), complementary with position 79–81, reduced translation to 85.4% of that of the wt. P2 (cgaaagc), complementary with position 79–85, reduced translation to 70.5% of that of the wt. P3 (agcttgggc) and P4 (cgaaagcttgggc) reduced translation to 44.4 and 40.6% of wt, respectively. P5 (agagacgaaagcttgggc) and P6 (gcgagaggagtaagagacgaaagc ttgggc) reduced translation to 23.8 and 16.5% of that of the wt, respectively (Figure 10A). These oligonucleotides were designed to be complementary with the bases, which are responsible for the long-distance RNA–RNA interaction or the dynamic tertiary equilibrium state. Three nucleotide base pairings from P1 reduced translation by 15% at 25°C. When the length was longer, the negative effect was increased (Figure 10A), which may be associated with the

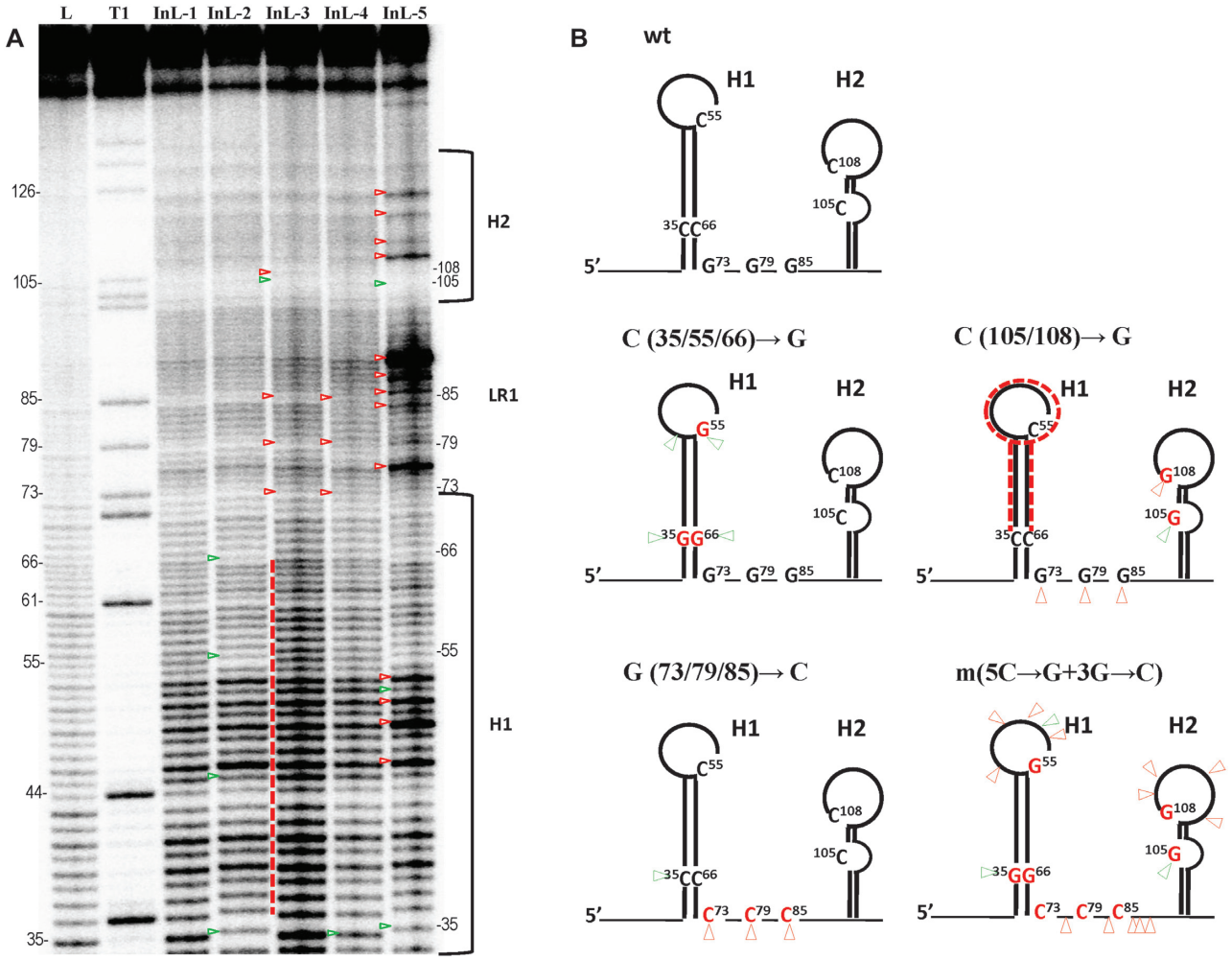

Figure 8. Structure probing of WYMV RNA1 5′-UTR or its mutants on discontinuous base-pairing cytosines (C) and guanines (G). (**A**) In-line probing of WYMV RNA1 5′-UTR or its mutants on discontinuous base pairing C and G. The legend is similar to that of Figure 2A. Red broken lines indicate the continuous stronger cleavage pattern. InL-1, RNA1 5′-UTR; InL-2: C(35/55/66)→G; InL-3,C(105/108)→G; InL-4, G(73/79/85)→C; InL-5, m(5C→G+3G→C). (**B**) RNA structure of WYMV RNA1 5′-UTR or its mutants. Red nucleotides indicate mutation sites. The red broken line indicates the continuous stronger cleavage pattern. Green hollow triangles point to the weaker cleavage sites, whereas red hollow triangles point to the stronger cleavage sites compared within corresponding sites in the wt RNA1 5′-UTR.

probability and dependability of base pairing at 25°C. The 13 or 9 nt oligonucleotides complementary with the loop of H1 also presented remarkable negative effects on translation, whereas the 13 or 9 nt oligonucleotides complementary with the outside region of core elements within the 5′-UTR only had slight effects on translation (Figure 10B and C). This competition assay from different oligonucleotides further confirmed the essential role of core elements, such as LR1 and the top loop of H1. It also provided a way to cure diseases caused by WYMV through inhibiting viral translation when similar agents could form base pairings with the core IRES elements of the 5′-UTR in WYMV RNA1.

DISCUSSION

A unique IRES with dynamic equilibrium state of the RNA tertiary structure in WYMV RNA 1 5′-UTR

IRESes are important elements by which RNA viruses and host cellular mRNA can facilitate cap-independent translation (10,16,17). In animal RNA viruses, six types of IRES have been identified based on their complicated structural characteristics and associated host factors (17,18). In plant RNA viruses, IRESes have been mainly identified in members of the Potyviridae family, whose genome architecture resembles that of the animal picornaviruses (16). However, IRESes in the Potyviridae family present remarkable differences in length and structural complexity from those in the Picornavirales order (16–18).

The identified cap-independent translation activity in members of the Potyviridae family is determined by their 60–190 nt 5′-UTR, which is far less than the length of animal picornaviral IRESes, which have at least 450 nt (16). Even for the newly identified TriMV with the 739 nt 5′-UTR, IRES activity mainly relies on the sequences of positions 442–709, which is also smaller than the length of animal picornaviral IRESes (58). In this study, the IRES activity of WYMV RNA1 was also determined by 162 nt 5′-UTR, especially within positions 20–130 (Supplementary

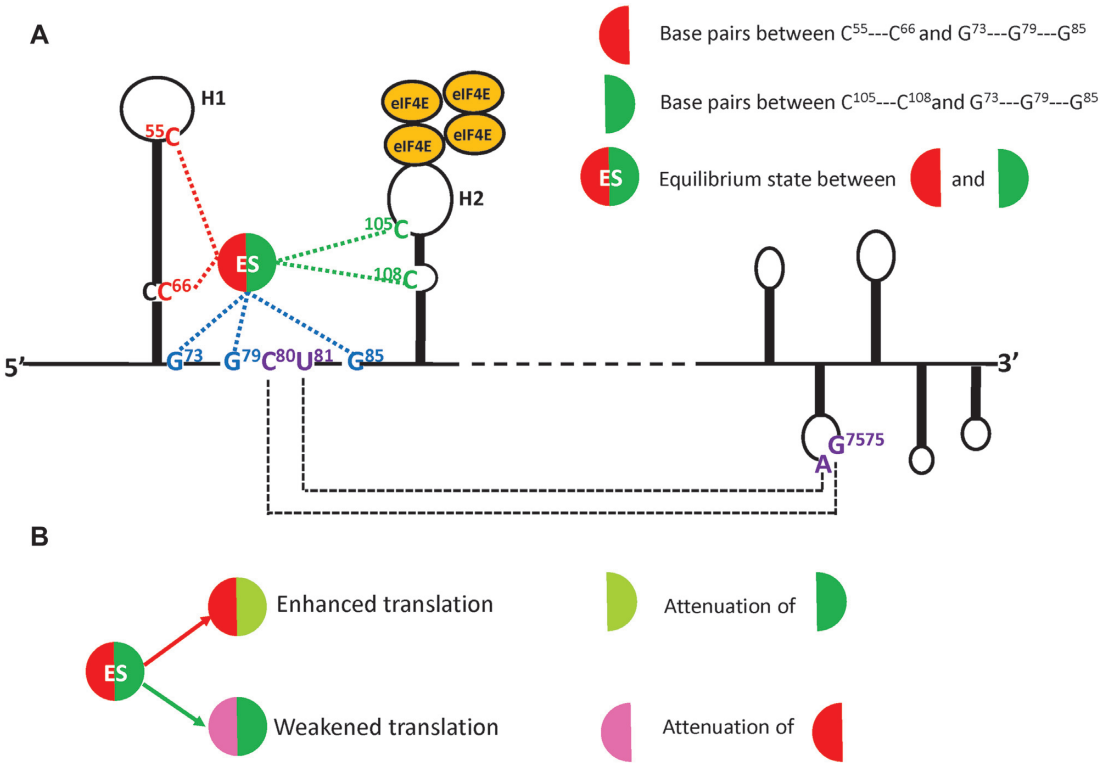

Figure 9. Characteristics of core *cis*-elements of IRES within 5′-UTRs of RNA1 of *WYMV*. (**A**) Core *cis*-elements of IRES within WYMV RNA1. Black broken lines indicate long-distance base pairs; H1, hairpin1; H2, hairpin 2; Red, green and blue broken lines indicate the dynamics equilibrium state (ES) of discontinuous base pairs among C^{55}, C^{66}, C^{105}, C^{108} and G^{73}, G^{79}, G^{85}. (**B**) Relationship between the variation tendency of ES and translation.

Figure S1) and additional coding sequences did not enhance the activity of the 5′-UTR in cap-independent translation (Figure 1). This study of WYMV IRES further strengthened the viewpoint that the length of the IRES in plant RNA viruses is shorter than that of animal picornaviral IRESes. These shorter IRESes in the Potyviridae family may be more coupled with their much larger VPg proteins (20–23 kDa) than with picornaviruses (2–3 kDa) (43). The VPg protein in potyviruses seems to be involved in translation through the interaction with cap-binding factors and ribosome proteins (59,60), whereas the VPgs of animal picornaviruses seem to be dispensable for their translation through unlinking from viral RNAs (61). The detailed relationship and function between VPg and IRESes in the cap-independent translation are still unclear.

Except for differences in the length of IRESes and VPg, the most remarkable difference between plant RNA and animal RNA viruses is the complexity of the IRES structure, which may be associated with the %GC content and △G (16). Most of the reported cap-independent translation elements in the 5′-UTR of the *P*otyviridae family seemed to be devoid of a stable secondary structure or present a weak secondary structure (16). There are few reports on the Potyviridae family being involved in the structural requirements for cap-independent translation enhancement. Two pseudoknots in the 5′leader are required for TEV to facilitate translation enhancement (62). The cap-independent translation enhancement of TriMV merely relied on an SL structure at position 469–490 within its unusually long 5′-UTR, although this long 5′-UTR presented a similar %GC content and △G as did animal picornavirus (16,58). However, previous reports on PVY suggested that the existence of the first SL structure in the 5′-UTR even prevent ribosomal scanning and inhibited translation (63). For WYMV, the %GC of the 5′-UTR in RNA1 (AF067124) is 48%, which is higher than that of other members of the Potyviridae family (16). However, the △G of the 5′-UTR in WYMV RNA1 (AF067124) is -21.29 kcal/mol, which is similar to that of other members of the Potyviridae family (16). This unique combination of high %GC and low △G of the short length 5′-UTR in WYMV RNA1 formed a unique IRES, which presents a tertiary structure maintained by several discontinuous C-G base pairs from two hairpins and their internal linker regions. Moreover, these discontinuous C-G base pairs have different roles in IRES activity. C-G base pairs between H1 and the linker region have positive effects on translation, whereas C-G base pairs between H2 and the linker region have negative effects on translation. The equilibrium state of the RNA tertiary structure in WYMV RNA1 5′-UTR subtly ensures a suitable level of the cap-independent translation.

The potential relationship between the equilibrium state of the IRES in WYMV RNA1 and local adaptation of WYMV in a single host

Wheat is the only natural host range of WYMV in the field. The unique method of transmission by fungus and the low-temperature replication model may limit the host range of WYMV (49–51). Emergence or host jumps for

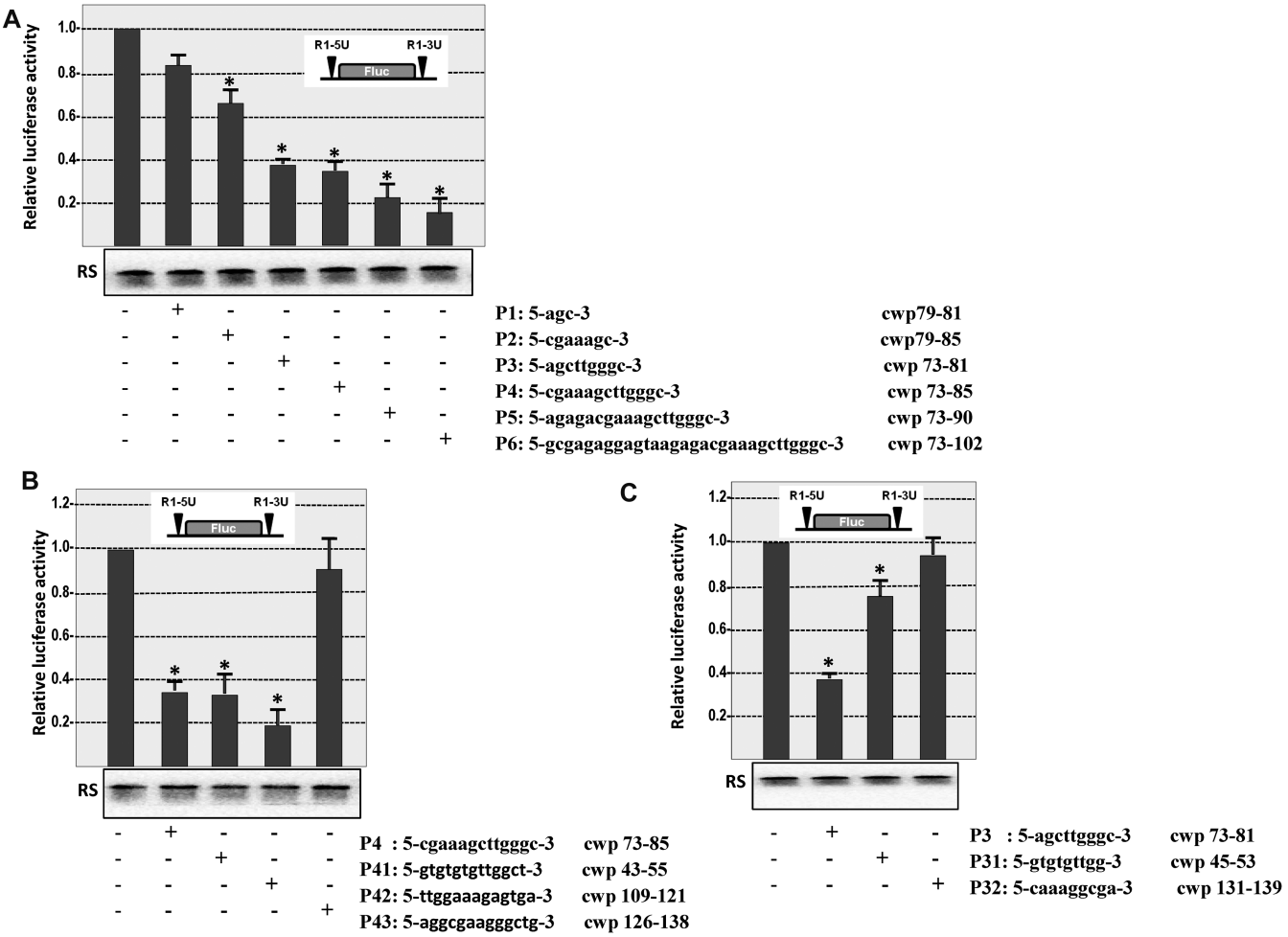

Figure 10. *Trans*-regulation of oligonucleotide on *in vitro* translation mediated by UTRs of WYMV RNA1. (**A**) *Trans*-regulation on translation from different length oligonucleotides complementary with the LR1 of WYMV RNA1 5′-UTR. cwp, complementary with the position. (**B**) *Trans*-regulation on translation from different 13 nt oligonucleotides complementary with the different regions of the 5′-UTR. (**C**) *Trans*-regulation on translation from different 9 nt oligonucleotides complementary with the different regions of the 5′-UTR. * indicates $P < 0.05$, ** $P < 0.01$, *** $P < 0.001$; RS indicates RNA stability assay after 1.5 h *in vitro* translation.

viruses require a complex interaction between the host population, vector and viruses through several phases of tradeoffs, including virus encounter of—and adaptation to—a new host, as well as long-term changes in virus epidemiology (64,65). WYMV presented several characteristics that adapt to wheat and ensure its subtle replication in wheat, the single host. One is the specific interaction between its VPg and the eIF4E of wheat, supported by the phenomenon wherein WYMV can infect previously non-susceptible barley when the barley contains the eIF4E from wheat (53). Another may be the equilibrium state of the IRES in WYMV RNA1, which ensures the translation fitness of WYMV RNA1 in wheat. The current wt IRES element in the 5′-UTRof WYMV RNA1 is not one that can enhance the cap-independent translation at the highest level. Any of the several mutations, including m7635, ML8, C105G and C108G, can remarkably increase the IRES activity, which implies that the current IRES in the RNA1 5′-UTR is involved in maintaining a suitable, but not the highest, level of cap-independent translation. It is suggested that robustness and not the maximum level of translation was the target of selection during the evolution of WYMV RNA1.

DATA AND SOFTWARE AVAILABILITY

Raw and processed data for luciferase activity have been deposited in the computer of the lab as a backup. Raw imaging data (e.g., uncropped, unannotated agarose gels, In-line probing and EMSA) corresponding to individual figure panels have been deposited in the computer of the lab as a backup.

SUPPLEMENTARY DATA

Supplementary Data are available at NAR Online.

ACKNOWLEDGEMENTS

We are grateful to Prof. Anne E. Simon (University of Maryland, USA), Prof. Shi-En LV (Mississippi State University, USA) and Xuguo Zhou (University of Kentucky,

USA) for valuable suggestions and critical modification on the manuscript.

FUNDING

National Natural Science Foundation of China [31872638, 31670147, 31370179]; Taishan Scholar Construction project [ts201712023]; Shandong 'Double Tops' Program [SYL2017XTTD11]. Funding for open access charge: National Natural Science Foundation of China [31872638].
Conflict of interest statement. None declared.

REFERENCES

1. Marcotrigiano,J., Gingras,A.C., Sonenberg,N. and Burley,S.K. (1997) Cocrystal structure of the messenger RNA 5′ cap-binding protein (eIF4E) bound to 7-methyl-GDP. *Cell*, **89**, 951–961.
2. Pestova,T.V., Lorsch,J.R. and Hellen,C.U.T. (2007) The mechanism of translation initiation in eukaryotes. In: MathewsMB, Soneberg,N and Hershey,JWB (eds). *Translational Control in Biology and Medicine*. Cold Spring Harbor Laboratory Press, NY, pp. 87–128.
3. Sonenberg,N. and Hinnebusch,A.G. (2009) Regulation of translation initiation in eukaryotes: mechanisms and biological targets. *Cell*, **136**, 731–745.
4. Gallie,D.R. (1998) A tale of two termini: a functional interaction between the termini of an mRNA is a prerequisite for efficient translation initiation. *Gene*, **216**, 1–11.
5. Kieft,J.S. (2008) Viral IRES RNA structures and ribosome interactions. *Trends Biochem. Sci.*, **33**, 274–283.
6. Nicholson,B.L. and White,K.A. (2011) 3′ Cap-independent translation enhancers of positive-strand RNA plant viruses. *Curr. Opin. Virol.*, **1**, 373–380.
7. Simon,A.E. and Miller,W.A. (2013) 3′ cap-independent translation enhancers of plant viruses. *Annu. Rev. Microbiol.*, **67**, 21–42.
8. Jackson,R.J., Hellen,C.U.T and Pestova,T.V. (2010) The mechanism of eukaryotic translation initiation and principles of its regulation. *Nat. Rev. Mol. Cell Biol.*, **11**, 113–127.
9. Danthinne,X., Seurinck,J., Meulewaeter,F., Montagu,M.V. and Cornelissenl,M. (1993) The 3′ untranslated region of satellite *Tobacco necrosis virus* RNA stimulates translation in vitro. *Mol. Cell Biol.*, **13**, 3340–3349.
10. Weingarten-Gabbay,S., Elias-Kirma,S., Nir,R., Gritsenko,A.A., Stern-Ginossar,N., Yakhini,Z., Weinberger,A. and Segal,E. (2016) Systematic discovery of cap-independent translation sequences in human and viral genomes. *Science*, **351**, 240–240.
11. Jang,S.K., Kräusslich,H.G., Nicklin,M.J., Duke,G.M., Palmenberg,A.C. and Wimmer,E. (1988) A segment of the 5′ nontranslated region of *Encephalomyocarditis virus* RNA directs internal entry of ribosomes during in vitro translation. *J. Virol.*, **62**, 2636–2643.
12. Pelletier,J. and Sonenberg,N. (1988) Internal initiation of translation of eukaryotic mRNA directed by a sequence derived from poliovirus RNA. *Nature*, **334**, 320–325.
13. Baird,S.D., Turcotte,M., Korneluk,R.G. and Holcik,M. (2006) Searching for ires. *RNA*, **12**, 1755–1785.
14. Ungureanu,N.H., Cloutier,M., Lewis,S.M., De Silva,N., Blais,J.D., Bell,J.C. and Holcik,M. (2006) Internal ribosome entry site-mediated translation of apaf-1, but not xiap, is regulated during uv-induced cell death. *J. Biol. Chem.*, **281**, 15155–15163.
15. Xue,S., Tian,S., Fujii,K., Kladwang,W. and Barna,M. (2014) Rna regulons in hox 5′ UTRs confer ribosome specificity to gene regulation. *Nature*, **517**, 33–38.
16. Zhang,J., Roberts,R. and Rakotondrafara,A.M. (2015) The role of the 5′ untranslated regions of Potyviridae in translation. *Virus Res.*, **206**, 74–81.
17. Lozano,G. and Martínez-Salas,E. (2015) Structural insights into viral IRES-dependent translation mechanisms. *Curr. Opin. Virol.*, **12**, 113–120.
18. Sweeney,T.R., Dhote,V., Yu,Y. and Hellen,C.U. (2012) A distinct class of internal ribosomal entry site in members of the Kobuvirus and proposed Salivirus and Paraturdivirus genera of the Picornaviridae. *J. Virol.*, **86**, 1468–1486.
19. Nakashima,N. and Uchiumi,T. (2009) Functional analysis of structural motifs in dicistroviruses. *Virus Res.*, **139**, 137–147.
20. Fernández,I.S., Bai,X.C., Murshudov,G., Scheres,S.H. and Ramakrishnan,V. (2014) Initiation of translation by cricket paralysis virus IRES requires its translocation in the ribosome. *Cell*, **157**, 823–831.
21. Belsham,G.J. and Jackson,R.J. (2000) Translation initiation on picornavirus RNA. In: Sonenberg,N, Hershey,JWB and Mathews,MB (eds). *Translational Control of Gene Expression*. Cold Spring Harbor Laboratory Press, Cold Spring Harbor, NY, pp. 869–900.
22. deBreyne,S., Yu,Y., Unbehaun,A., Pestova,T.V. and Hellen,C.U.T. (2009) Direct functional interaction of initiation factor eIF4G with type 1 internal ribosomal entry sites. *Proc. Natl. Acad. Sci. U.S.A.*, **106**, 9197–9202.
23. Niepmann,M. (2009) Internal translation initiation of picornaviruses and *Hepatitis C virus*. *Biochim. Biophys. Acta*, **1789**, 529–541.
24. Hollister,J.R., Vagnozzi,A., Knowles,N.J. and Rieder,E. (2008) Molecular and phylogenetic analyses of bovine rhinovirus type 2 shows it is closely related to foot-and-mouth disease virus. *Virology*, **373**, 411–425.
25. Kolupaeva,V.G., Lomakin,I.B., Pestova,T.V. and Hellen,C.U. (2003) Eukaryotic initiation factors 4G and 4A mediate conformational changes downstream of the initiation codon of the encephalomyocarditis virus internal ribosomal entry site. *Mol. Cell Biol.*, **23**, 687–698.
26. Yu,Y., Abaeva,I.S., Marintchev,A., Pestova,T.V. and Hellen,C.U.T. (2011) Common conformational changes induced in type 2 picornavirus IRESes by cognate trans-acting factors. *Nucleic Acids Res.*, **39**, 4851–4865.
27. Brown,E.A., Zajac,A.J. and Lemon,S.M. (1994) In vitro characterization of an internal ribosomal entry site (IRES) present within the 5′ nontranslated region of *Hepatitis A virus* RNA: comparison with the IRES of *Encephalomyocarditis virus*. *J. Virol.*, **68**, 1066–1074.
28. Ali,I.K., McKendrick,L., Morley,S.J. and Jackson,R.J. (2001) Activity of the *Hepatitis A virus* IRES requires association between the cap-binding translation initiation factor (eIF4E) and eIF4G. *J. Virol.*, **75**, 7854–7863.
29. Yi,M.K., Schultz,D.E. and Lemon,S.M. (2000) Functional significance of the interaction of hepatitis A virus RNA with glyceraldehyde 3-phosphate dehydrogenase (GAPDH): opposing effects of GAPDH and polypyrimidine tract binding protein on internal ribosome entry site function. *J. Virol.*, **74**, 6459–6468.
30. Lukavsky,P.J. (2009) Structure and function of HCV IRES domains. *Virus Res.*, **139**, 166–171.
31. Kieft,J.S., Zhou,K., Jubin,R. and Doudna,J.A. (2001) Mechanism of ribosome recruitment by hepatitis C IRES RNA. *RNA*, **7**, 194–206.
32. Filbin,M.E., Vollmar,B.S., Shi,D., Gonen,T. and Kieft,J.S. (2013) HCV IRES manipulates the ribosome to promote the switch from translation initiation to elongation. *Nat. Struct. Mol. Biol.*, **20**, 150–158.
33. Hashem,Y., Des Georges,A., Dhote,V., Langlois,R., Liao,H. Y., Grassucci,R. A. and Frank,J. (2013) Hepatitis-C-virus-like internal ribosome entry sites displace eIF3 to gain access to the 40S subunit. *Nature*, **503**, 539–543.
34. Seth,P.P., Miyaji,A., Jefferson,E.A., Sannes-Lowery,K.A., Osgood,S.A., Propp,S.S., Ranken,R., Massire,C., Sampath,R. and Ecker,D.J. (2005) SAR by MS: discovery of a new class of RNA-binding small molecules for the *Hepatitis C virus*: internal ribosome entry site IIA subdomain. *J. Med. Chem.*, **48**, 7099–7102
35. Gasparian,A.V., Neznanov,N., Jha,S., Galkin,O., Moran,J.J., Gudkov,A.V. and Komar,A.A. (2010) Inhibition of *encephalomyocarditis virus* and poliovirus replication by quinacrine: implications for the design and discovery of novel antiviral drugs. *J. Virol.*, **84**, 9390–9397.
36. Liu,S., Nelson,C.A., Xiao,L., Lu,L., Seth,P.P., Davis,D.R. and Hagedorn,C.H. (2011) Measuring antiviral activity of benzimidazole molecules that alter IRES RNA structure with an infectious *Hepatitis C virus* chimera expressing Renilla luciferase. *Antiv. Res.*, **89**, 54–63
37. Dibrov,S.M., Ding,K., Brunn,N.D., Parker,M.A., Bergdahl,B.M., Wyles,D.L. and Hermann,T. (2012) Structure of a *Hepatitis C virus* RNA domain in complex with a translation inhibitor reveals a

binding mode reminiscent of riboswitches. *Proc. Natl. Acad. Sci. U.S.A.*, **109**, 5223–5228.
38. Boerneke,M.A., Dibrov,S.M., Gu,J., Wyles,D.L. and Hermann,T. (2014) Functional conservation despite structural divergence in ligand-responsive RNA switches. *Proc. Natl. Acad. Sci. U.S.A.*, **111**, 15952–15957
39. Lozano,G., Trapote,A., Ramajo,J., Elduque,X., Grandas,A., Robles,J. and Martínez-Salas,E. (2015) Local RNA flexibility perturbation of the IRES element induced by a novel ligand inhibits viral RNA translation. *RNA Biol.*, **12**, 555–568.
40. Carrington,J.C. and Freed,D.D. (1990) Cap-independent enhancement of translation by a plant potyvirus 5′ nontranslated region. *J. Virol.*, **64**, 1590–1597.
41. Basso,J., Dallaire,P., Charest,P.J., Devantier,Y. and Laliberte,J.F. (1994) Evidence for an internal ribosome entry site within the 5′ non-translated region of turnip mosaic potyvirus RNA. *J. Gen. Virol.*, **75**, 3157–3165.
42. Levis,C. and Astier-Manifacier,S. (1993) The 5′ untranslated region of PVY RNA, even located in an internal position, enables initiation of translation. *Virus Genes*, **7**, 367–379.
43. Jiang,J. and Laliberté,J.F. (2011) The genome-linked protein VPg of plant viruses—a protein with many partners. *Curr. Opin. Virol.*, **1**, 347–354.
44. Khan,M.A., Miyoshi,H., Gallie,D.R. and Goss,D.J. (2008) Potyvirus genome-linked protein, VPg, directly affects wheat germ in vitro translation: interactions with translation initiation factors eIF4F and eIFiso4F. *J. Biol. Chem.*, **283**, 1340–1349.
45. Khan,M.A. and Goss,D.J. (2012) Poly(A)-binding protein increases the binding affinity and kinetic rates of interaction of viral protein linked to genome with translation initiation factors eIFiso4F and eIFiso4F·4B complex. *Biochemistry*, **51**, 1388–1395.
46. Namba,S., Kashiwazaki,S., Lu,X., Tamura,M. and Tsuchizaki,T.(1998) Complete nucleotide sequence of wheat yellow mosaic by movirus genomic RNAs. *Arch. Virol.*, **143**, 631–643.
47. Chen,J., Sohn,A., Chen,J.P., Lei,J., Cheng,Y., Schulze,S., Steinbiss,H.H., Antoniw,J.F. and Adams,M.J. (1999) Molecular comparisons amongst wheat bymovirus isolates from Asia, North America and Europe. *Plant Pathol.*, **48**, 642–647.
48. Yu,J., Yan,L., Su,N., Huo,Z., Li,D., Han,C., Yang,L., Cai,Z. and Liu,Y.(1999) Analysis of nucleotide sequence of *Wheat yellow mosaic virus* genomic RNAs. *Sci. China*, **42**, 554–560.
49. Wang,X., Liu,Y., Han,C., Wu,Y. and Zhao,Z. (2010) Present situation and development strategies for the research and control of wheat viral diseases (in Chinese). *Plant Protection*, **36**, 13–19.
50. Lin,M. and Ruan,Y. (1986) A study on *Wheat yellow mosaic virus* (in Chinese). *Acta Phytopathol. Sin.*, **16**, 73–78.
51. Hariri,D., Courtillot,M., Zaoui,P. and Lapierre,H. (1987) Multiplication of *Soilbornewheat mosaic virus* (SBWMV) in wheat roots infected by a soil carrying SBWMV and *Wheat yellow mosaic virus*. *Agronomie*, **7**, 789–796.
52. Li,D., Yan,L., Su,N., Han,C., Hou,Z., Yu,J. and Liu,Y. (1999) The nucleotide sequence of a Chinese isolate of *Wheat yellow mosaic virus* and its comparison with a Japanese isolate. *Arch.Virol.*, **144**, 2201–2206
53. Li,H. and Shirako,Y. (2015) Association of VPg and eIF4E in the host tropism at the cellular level of *Barley yellow mosaic virus* and *Wheat yellow mosaic virus* in the genus Bymovirus. *Virology*, **476**, 159–167.
54. Geng,G., Yu,C., Wang,D., Gu,K., Shi,K., Li,X., Tian,Y. and Yuan,X. (2017) Evolutional analysis of two new isolates of *Wheat yellowmosaic virus* from Shandong Province, China (in Chinese). *Acta Phytopathol. Sinica*, **47**, 348–356.
55. Wang,D., Yu,C., Liu,S., Wang,G., Shi,K., Li,X. and Yuan,X. (2017) Structural alteration of a BYDV-like translation element (BTE) that attenuates p35 expression in three mild *Tobacco bushy top virus* isolates. *Sci. Rep.*, **7**, 4213.
56. George,D. and Mallery,P. (2016) *IBM SPSS Statistics 23 Step by Step: A Simple Guide and Reference*. Routledge, NY and OX.
57. Yuan,X., Shi,K. and Simon,A.E. (2012) A local, interactive network of 3′ RNA elements supports translation and replication of *Turnip crinkle virus*. *J. Virol.*, **86**, 4065–4081.
58. Roberts,R., Zhang,J., Mayberry,L.K., Tatineni,S., Browning,K.S. and Rakotondrafara,A.M. (2015) A unique 5′ translation element discovered in *Triticum mosaic virus*. *J. Virol.*, **89**, 12427–12440.
59. Eskelin,K., Hafren,A., Rantalainen,K.I. and Makinen,K. (2011) PotyviralVPg enhances viral RNA translation and inhibits reporter mRNA translation in planta. *J. Virol.*, **85**, 9210–9221.
60. Wang,A. and Krishnaswamy,S. (2012) Eukaryotic translation initiation factor 4E-mediated recessive resistance to plant viruses and its utility in crop improvement. *Mol. Plant Pathol.*, **13**, 795–803
61. Langereis,M.A., Feng,Q., Nelissen,F.H., Virgen-Slane,R., van der Heden van Noort,G.J., Maciejewski,S., Filippov,D.V., Semler,B.L., van Delft,F.L. and van Kuppeveld,F.J. (2014) Modification of picornavirus genomic RNA using 'click' chemistry shows that unlinking of the VPg peptide is dispensable for translation and replication of the incoming viral RNA. *Nucleic Acids Res.*, **42**, 2473–2482.
62. Zeenko,V. and Gallie,D.R. (2005) Cap-independent translation of *Tobacco etch virus* is conferred by an RNA pseudoknot in the 5′-leader. *J. Biol. Chem.*, **280**, 26813–26824.
63. Yang,L.J., Hidaka,M., Sonoda,J., Masaki,H. and Uozumi,T. (1997) Mutational analysis of the *Potato virus Y* 5′ untranslated region for alteration in translational enhancement in tobacco protoplasts. *Biosci. Biotechnol. Biochem.*, **61**, 2131–2133.
64. Elena,S.F., Fraile,A. and García-Arenal,F. (2014) Evolution and emergence of plant viruses. *Adv. Virus Res.*, **88**, 161–191.
65. Elena,S.F. (2017) Local adapation of plant viruses: lessons from experimental evolution. *Mol. Ecol.*, **26**, 1711–1719.